Dewetting rates of thin liquid films

Dewetting rates of thin liquid films

A Münch[1]

Humboldt University in Berlin, Faculty of Mathematics and Natural Sciences II, Institute of
Mathematics, 10099 Berlin, Germany

E-mail: muench@mathematik.hu-berlin.de

Abstract
We investigate the dewetting rates of thin liquid films using a lubrication
model that describes the dewetting process of polymer melts on hydrophobized
substrates. We study the effect of different boundary conditions at the
liquid/solid interface, in particular, of the no-slip and the Navier slip boundary
condition, and compare our numerical solutions for the no-slip and the slip-
dominated cases to available results that originate from scaling arguments,
simplified flow assumptions and energy balances. We furthermore consider
these issues for an extended lubrication model that includes nonlinear curvature.

1. Introduction

Liquid, viscous films that are uniformly spread onto a hydrophobic surface tend to dewet in
a process that is initiated either spontaneously through spinodal decomposition or induced
for example through nucleation. The dry spots, or holes, that form as a result subsequently
grow as the newly formed contact line recedes, thereby accumulating liquid in a characteristic
capillary ridge at the edge of the hole, which increases in width and height as the dewetting
proceeds. The growth of a hole continues until it gets close to neighbouring holes. The liquid
evolves into a pattern of droplets and possibly ridges where holes have met; eventually, these,
too, break up into droplets. The droplet pattern continues to change on a long timescale in a
process called coarsening, whereby drops slowly drift and exchange mass.

Various aspects of these stages have been addressed experimentally and theoreti-
cally [8, 9, 11, 17, 20, 25, 26, 28]. Theoretical and in particular numerical work using lu-
brication models for the film profile have mostly concentrated on the process of the initial
hole formation [25, 26], or the formation of multiple hole patterns and of satellite holes on the
side facing the 'thick' film [1, 12] and also on the long time evolution of the residual droplet
patterns [4]. Except for the no-slip case [3], the evolution of a single hole after rupture but
well before the collision with neighbouring holes and the growth and shape of the ridges has

[1] Address for correspondence: Weierstrass Institute for Applied Analysis and Stochastics (WIAS), Mohrenstraße 39,
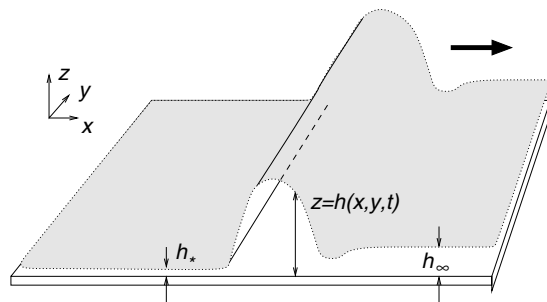10117 Berlin, Germany.

Figure 1. Sketch of a portion of a dewetting polymer film of initial thickness h_∞. The dewetting front and the ridge propagate in the direction of the positive x-axis, as indicated by the bold-face arrow, leaving behind a residual film of thickness h_*.

only been treated using approximate formulas derived from scaling arguments and energy balances ([2, 7, 15] and references therein). In order to understand the dynamics in this regime, it is first of all of interest to establish how these approximated laws compare to the solution of the corresponding lubrication model, essentially a fourth order nonlinear PDE for the film profile.

This task has been carried out in considerable detail by Ghatak *et al* [3] for the case where a no-slip condition holds at the liquid/solid interface. For the Navier slip boundary condition, no comparable study exists. The focus of this paper is the comparison of our numerical solutions for the evolution of the contact line position for a lubrication model with the predictions of the scaling laws. Furthermore, we also consider extensions of the lubrication model where the full nonlinear expression for the curvature of the liquid surface replaces the Laplacian that is common in lubrication theory. This is important for applications where the solid is very hydrophobic, leading to large contact angles that violate, at least locally, the small slope assumption.

2. Formulation

In order to describe the evolution of the film surface $z = h(x, y, t)$ we use a lubrication model that includes the influence of surface tension and the effective interface potential W of the air/polystyrene/SiO/Si layer system used in [22]. Figure 1 shows the film as it dewets in the x-direction from a straight front oriented in the y-direction. In dimensional form, the lubrication model [14], which we state here for the one-dimensional case, since we will not consider spanwise perturbations in this paper, reads

$$3\eta h_t + \frac{\partial}{\partial x}\left[m(h)\left(\sigma h_{xxx} - W''(h)h_x\right)\right] = 0, \tag{1}$$

where η and σ are the liquid viscosity and the liquid surface tension, respectively, and $W''(h)$ is the second derivative of the effective interface potential with respect to h.

Also, $m(h)$ is a non-negative mobility coefficient, the form of which depends on the boundary conditions at the liquid/solid interface. The widely used Navier slip condition relates the slippage velocity v of the liquid at the wall to the local shear rate $\partial v/\partial z$ via

$$v = \beta\,\partial v/\partial z, \tag{2}$$

where the slip length β is defined as the distance below the interface at which the liquid velocity extrapolates to zero. For the above slip boundary condition at the substrate, the mobility has the form $m(h) = h^3 + \beta h^2$.

The effective interface potential is composed of repulsive and attractive long-range van der Waals contributions, with a separate contribution for each of the layers of the substrate, and a short-range term which accounts for Born-type repulsion. The latter term provides a cut-off by penalizing a thinning of the film below a positive thickness threshold given by the minimum h_* of the potential. In the specific experimental situation, the substrate is a Si wafer coated with a native SiO layer of thickness d_{SiO}, in turn covered by a monolayer of OTS of thickness d_{OTS}. The effective potential for this situation as given in [23] is

$$W(h) = \frac{c_{\mathrm{s}}}{h^8} - \frac{A_{\mathrm{OTS}}}{12\pi h^2} + \frac{A_{\mathrm{OTS}} - A_{\mathrm{SiO}}}{12\pi(h + d_{\mathrm{OTS}})^2} + \frac{A_{\mathrm{SiO}} - A_{\mathrm{Si}}}{12\pi(h + d_{\mathrm{OTS}} + d_{\mathrm{SiO}})^2} \qquad (3)$$

where c_{s} denotes the strength of the short-range part of the potential, and A_{SiO}, A_{Si} and A_{OTS} are the Hamaker constants of polystyrene on SiO, Si and OTS respectively. A_{OTS} and A_{SiO} nearly cancel out, so we can neglect the third term in what follows.

The numerical values for (3) were constructed in [23] based on AFM measurements of the static contact angle of about $58.5°$. This means that slopes near the contact line are order one, so that it becomes interesting to consider replacing the linearized curvature in (1) with the full nonlinear expression. We therefore also investigate here a modified model

$$3\eta h_t + \frac{\partial}{\partial x}\left[m(h)\left(\sigma\kappa_x - W''(h)h_x \right) \right] = 0, \qquad \kappa = \frac{h_{xx}}{(1 + h_x^2)^{3/2}}, \qquad (4)$$

and compare the results with those for (1). Augmented lubrication models like (4) that retain the full nonlinear curvature have been used for various types of coating flows and for the case of liquids spreading on solids, for example in [27].

The lubrication model (1) treats the polymer film in its melt state as a Newtonian liquid. The assumption of Newtonian behaviour is justified for polymers having short chains well below the entanglement length of polystyrene (which is around $18\ \mathrm{kg\ mol^{-1}}$ [13]) in studies by [6, 12, 21]. Our study will focus on this case.

In order to minimize the number of parameters that appear in the equation, we non-dimensionalize so that the time derivative of h, the contribution from surface tension and the first terms in $W''(h)h_x$ balance. This is achieved with the following choices:

$$H = \left(\frac{144\pi c_{\mathrm{s}}}{A_{\mathrm{SiO}}}\right)^{\frac{1}{6}}, \qquad L = 4\pi\left(\frac{81\sigma^3 c_{\mathrm{s}}^2}{2\pi A_{\mathrm{SiO}}^5}\right)^{\frac{1}{6}}, \qquad T = \frac{864\pi^2\eta\sigma}{A_{\mathrm{SiO}}^2}\left(\frac{4\pi^5 c_{\mathrm{s}}^5}{9A_{\mathrm{SiO}}^5}\right)^{\frac{1}{6}} \qquad (5)$$

for the normal and parallel length scales and for the timescale. Introducing these scalings for h, x, y and for t we obtain

$$\frac{\partial h}{\partial t} + \frac{\partial}{\partial x}\left[m(h)\left(h_{xxx} - \left\{ \frac{1}{h^{10}} - \frac{1}{h^4} + \frac{a}{(h + d)^4} \right\} h_x \right) \right] = 0. \qquad (6)$$

Note that in (6) the slip length β, which is contained in the mobility $m(h)$, has also been scaled with H. The expression in curly brackets is the second derivative of the following non-dimensional form of the effective interface potential:

$$W(h) = \frac{1}{72h^8} - \frac{1}{6h^2} + \frac{a}{6(h + d)^2}, \qquad (7)$$

which contains two parameters, namely

$$a = (A_{\mathrm{SiO}} - A_{\mathrm{Si}})/A_{\mathrm{SiO}} \qquad \text{and} \qquad d = (d_{\mathrm{OTS}} + d_{\mathrm{SiO}})/H. \qquad (8)$$

For the model (4) with the nonlinear expression for curvature, the corresponding non-dimensional form is

$$\frac{\partial h}{\partial t} + \frac{\partial}{\partial x}\left[m(h)\left(\kappa_x - W''(h)h_x \right) \right] = 0, \qquad \kappa = \frac{h_{xx}}{(1 + \rho^2 h_x^2)^{3/2}}, \qquad (9)$$

Table 1. List of physical parameters, scalings and non-dimensional parameters (note $d_\Sigma \equiv d_{\text{OTS}} + d_{\text{SiO}}$).

c_s	4×10^{-81} J m^6	A_{SiO}	2.2×10^{-20} J	A_{Si}	-1.4×10^{-19} J
d_Σ	4.4×10^{-9} m	σ	30.8×10^{-3} N m^{-1}	η	4×10^4 Pa s
H	2.09×10^{-10} m	L	1.29×10^{-10} m	T	1.19×10^{-4} s
a	7.36	d	21.1	ρ	1.62

where ρ is another parameter that measures the ratio of the length scales,

$$\rho = \frac{H}{L} = \frac{1}{2} \left(\frac{A_{\text{SiO}}^4}{18\pi^4\sigma^3 c_s} \right)^{1/2}.$$

The numerical experiments presented here are based on physical parameters from [23, 9] which are listed in table 1, together with the resulting values for the scalings and for the non-dimensional parameters a, d and ρ. Note that the length scales are very small (in the sub-nanometric range) which is to be expected since the balance we used to fix them includes the Born repulsion term in the potential which acts only over very small distances. As a result, the residual film $h_* = 0.833$ (equivalent to 0.174 nm) is an order one value in the scaled variables, while the size of the ridge or the distance it travels will have very large values.

In many fluid mechanical situations, the slip length is very small compared to other length scales in the problem and slip conditions such as (2) are only invoked to relax the stress singularity near a moving three-phase contact line [5]. Since the inclusion of a Born repulsion term in the potential $W(h)$ stabilizes a very thin residual film in the region of the hole, thus regularizing the contact-line region, one might consider neglecting slip altogether and set $\beta = 0$. There is growing evidence, however, that polymer melts can slip significantly at the substrate, i.e. the slip length β can be on the order of ten to a few hundred nanometres, or even larger (e.g. [16, 24]). The slip length then becomes comparable to, or even exceeds, the thickness of the polymer film used in many experiments, for example those in [7, 11]. Then one would expect that the term βh^2 balances or dominates h^3 in the mobility and in fact in the latter case determines the timescale of the evolution. In the following, we will discuss and compare the two asymptotic cases: no slip, where $\beta = 0$ so that $m(h) = h^3$, and the (Navier) slip-dominated case with mobility $m(h) = h^2$. The latter is obtained by rescaling time with β, and letting $\beta \to \infty$ in (6) and (9). We note that this limit was considered before for the lubrication model of a thin film by Sharma and Khanna in [24]. Finally, we also briefly look into the transition between these two regimes by using finite, non-zero values for β and observing the contact-line motion as the height of the ridge of the film profile approaches and then passes β.

3. Dewetting of the unperturbed ridges

To investigate the evolution of the straight ridge/dewetting front, we solve (6) numerically, and subsequently also (9), using a finite-difference scheme with implicit time discretization. The profile employed as initial condition is a steep front connecting the dewetted region and the unperturbed film of thickness h_∞, so that $\lim_{x \to -\infty} h = h_*$ and $\lim_{x \to \infty} h = h_\infty$. For the numerical experiments here, we usually set h_∞ to a reference value, $h_{\text{ref}} = 20.8$ (noting in passing that this is $25h_*$), and, where stated explicitly, to exactly the fourfold thickness. Recall that h_* is the film thickness that corresponds to the minimum of the potential (7) and is energetically strongly preferred compared to the initial thickness, so that in the computations the film dewets, i.e. the front moves to the right.

We remark that our choice for h_∞ corresponds to a dimensional film thickness of 4.34 nm. This is much smaller than the typical values used for the experiments presented in [9], which were in the range of 100 nm and more. However, larger values for h_∞ increase the computational work considerably, so we chose a value that was fairly small but large enough to prevent or delay satellite hole formation in the simulations until the ridge, i.e. the base state, had travelled over a distance that is comparable to typical experiment hole sizes. Satellite holes as described in [12] tend to form fairly quickly in thinner films through rupture of the first minimum of the oscillatory tail on the 'wet' side of the ridge. By this term we denote the side that faces the 'thick' film into which the ridge penetrates as it dewets.

We use the lubrication model in the no-slip and slip-dominated case to track the position of the front $x_c(t)$, which we take to be the location of the inflection point, on the 'dry' side of the ridge, i.e. the side that faces the dewetted area. This is where the dewetting front begins to pass over into the residual film in the hole and it captures quite well the place where one would intuitively place the contact line position. The results were normalized by subtracting the initial location of the front so that $x_c(0) = 0$. We then fit the ansatz

$$x_c(t) = a_0 + a_1 |t + a_2|^\lambda, \qquad \lambda > 0, \tag{10}$$

to the numerically obtained results for $x_c(t)$. Computations are continued, for each case, until the normalized $x_c(t)$ has reached 4.5×10^5, or 58 μm, and the data accumulated in this time are used to fit (10). Note that these (non-dimensional) times are different for the no-slip and the slip-dominated case, since the two mobilities $m(h) = h^3$ and $m(h) = h^2$ differ by a factor h that is typically equal or larger than h_∞ in the ridge and the thick film. To limit the effect of initial transients peculiar to our choice of initial data, we also limit the range of x_c for the fit from below in that we exclude all data points with $x_c < 1000$.

3.1. The no-slip case

We begin with a discussion of the no-slip case. Theoretical work (see [15] and references therein) predicts that, except for a logarithmic prefactor, the dewetting rates are independent of the size of the ridge, which would mean that the front moves at a constant speed, implying a spreading law like (10) with λ set to one. A best fit of (10) to the numerical results with $x_c \leqslant 4.5 \times 10^5$ for yields $\lambda = 0.913 < 1$, however. Such a deviation of the exponent from one was also noted in [3]. The authors also point out that increasing the time interval over which the fit is carried out tends to increase λ, suggesting that the predicted asymptotic behaviour might be approached eventually, but only for extremely long times.

Furthermore, dewetting rates are predicted to be independent of the initial thickness h_∞ of the dewetting film, see again [16] and references therein, and this is recovered to a good degree by our numerical computations for the lubrication model, see figure 2(a), though a slight difference remains.

The reason for the less than linear dewetting law can be routed to the logarithmic prefactor, which introduces a weak dependence on the width of the ridge [15]. Since the width of the ridge changes by orders of magnitude in the above numerical experiment, even a logarithmic dependence can have a noticeable effect on the observed front evolution. Furthermore, since the rates at which the size of the ridge grows depends on the initial film thickness h_∞, this provides a mechanism by which a (weak) dependence of the dewetting rates on h_∞ enters.

We can use the expression given in [15] for the dewetting velocity

$$\dot{x}_c(t) = \frac{1}{12 \times 2^{1/2} l} \frac{\sigma}{\eta} \theta_s^3,$$

to obtain a better fit function for x_c. Here $l \approx \ln(cw(t))$ denotes the logarithmic prefactor, $w(t)$ is the width of the ridge and c is a constant that depends on the (dynamical) contact angle and a
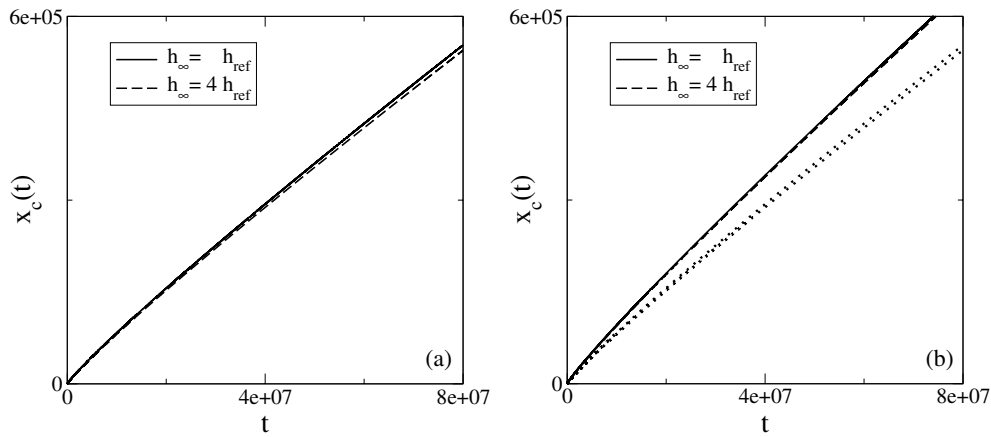
Figure 2. Evolution of the contact line position with time for the *no-slip* case, for two different values of h_∞. Panel (a) on the left shows the results for the linearized expression for curvature; the right panel shows the results using the full nonlinear expression for curvature. Note that dotted curves in (b) duplicate the solid and dashed curves from (a) to facilitate comparison of the results for the two curvature expressions.

microscopic length that provides a cut-off at the contact line (an obvious candidate here would be the residual film thickness h_*). We will not need a detailed expression for this constant in what follows, and also, further constant factors that appear will be tacitly absorbed into c.

Upon rescaling the expression, we obtain the following non-dimensional form:

$$\dot{x}_c(t) = \frac{\theta_s^3}{2^{5/2} \ln (cw(t))}. \tag{11}$$

The width can be approximately determined from the contact line evolution in the following way: as the ridge translates to the right its volume increases by $\dot{x}_c(t)h_\infty$. Furthermore, we assume that the ridge grows in approximately a self-similar way, so its volume scales like the product of its height and width. Assuming further that the dynamical contact angle remains constant [15] (noting though that for example in [3] it does change, but only slowly for later times), it follows that the ratio of the ridge height and width remains approximately constant, too. Hence the volume change is proportional to the time derivative of $w(t)^2$. Equating the two expressions for the increase in volume suggests that $w(t)$ is proportional to $(x_c(t)+c_1)^{1/2}$, where c_1 is another constant that we will not elaborate on.

Inserting into (11), we obtain

$$\dot{x}_c(t) = \frac{\theta_s^3}{2^{3/2} \ln (c(x_c(t) + c_1))},$$

which has the implicit solution

$$t = -t_0 + 2^{3/2}\theta_s^{-3}(x_c + c_1) \ln (c(x_c + c_1)), \tag{12}$$

where t_0 is a constant of integration. This suggests using the following function to fit with the numerical data for $x_c(t)$:

$$t = b_0 + b_1|x_c + b_3| \ln(b_2|x_c + b_3|), \qquad b_2 > 0. \tag{13}$$

Indeed, this ansatz could be excellently fitted to the numerical data in the range $1000 \leqslant x_c \leqslant 4.5 \times 10^5$, while a simple fit with a linear function produced a line that visibly differed from the numerical graph for $x_c(t)$. Moreover, we can compare the value obtained for b_1 with the
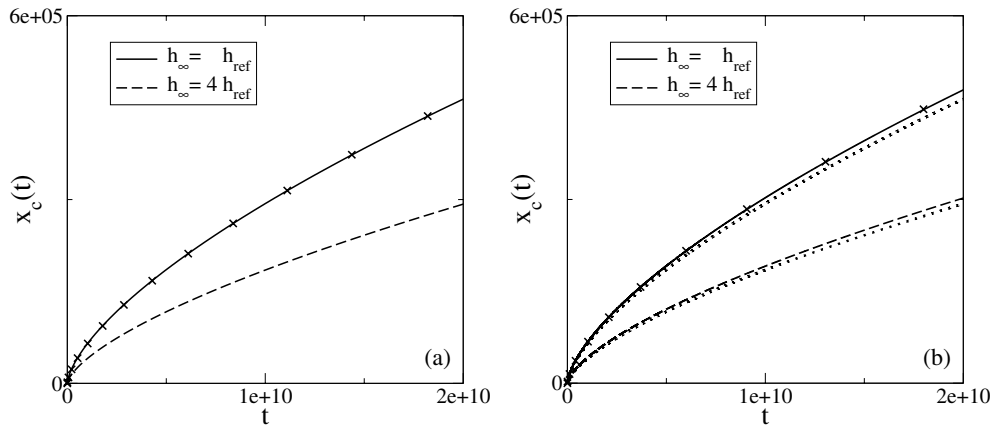
Figure 3. Evolution of the contact line position with time for the *slip-dominated* case, for two different values of h_∞. Panel (a) on the left shows the results for the linearized expression for curvature; the right panel shows the results using the full nonlinear expression for curvature. The dotted curves in (b) duplicate the solid and dashed curves from (a) to facilitate comparison of the results for the two curvature expressions. Note also that in each figure the crosses were obtained by rescaling the dashed curve with $4^{1/3}$.

theoretical prediction in (12). We interpret the static contact angle θ_s to actually mean the slope for the outer solution of a static ridge, which is given by $(-2W(h_*))^{1/2} = 0.596$ (see for example [4]); then we obtain $2^{3/2}\theta_s^{-3} = 13.4$. The fit resulted, for $h_\infty = h_{ref}$, in $b_1 = 13.3$, which is indeed close to the prediction.

Next we investigate the effect of retaining the full nonlinear curvature on the evolution of the front, by carrying out the corresponding numerical simulations for (9). We see in figure 2(b) that the evolution is closer to a linear law than for the model (6), i.e., the curves appear to be flatter and fitting of (10) results in a value for $\lambda = 0.919$ that is slightly closer to one. Again, a logarithmic ansatz (13) could be excellently fitted to the numerical data; taking as usual the results for $h_\infty = h_{ref}$, the fit yields $b_1 = 10.4$. Also, changing the film thickness has a smaller impact on the dewetting rate than for (6), as can be seen from comparing the solid and dashed curves in figure 2(b), which are closer together than in figure 2(a).

3.2. The slip-dominated case

For the slip-dominated case, [2, 16] predict a $t^{2/3}$ law for the evolution of the dewetting front. In fact, the evolution law is much more specific; in the form published by [18], it reads

$$x_c(t) = 2^{-4/3}C^{1/6}\sigma^{2/3}\theta_s^{5/3}\eta^{-2/3}h_\infty^{-1/3}\beta^{2/3}t^{2/3}$$

in dimensional form, from which we obtain the dimensionless version (by using (5) and then rescaling time according to $\beta t \to t$),

$$x_c(t) = \left[3^{2/3}C^{1/3}/4^{2/3}\right]\theta_s^{5/3}h_\infty^{-1/3}t^{2/3}. \tag{14}$$

We remark that since θ_s measures a slope, it also has been scaled by H/L. The value for the constant C is given by [18] to be about 0.1; using this, the numerical prefactor enclosed by brackets in (14) evaluates to 0.38.

We first verify the exponent for the dewetting law. A best fit of (10) to the numerically obtained evolution of $x_c(t)$ yields $\lambda = 0.661$, which is indeed very close to the prediction $\lambda = 2/3$. Also, (14) implies that for thicker initial coatings, the dewetting proceeds more slowly and in figure 3(a) we see that this is the case. In fact, upon rescaling the line for
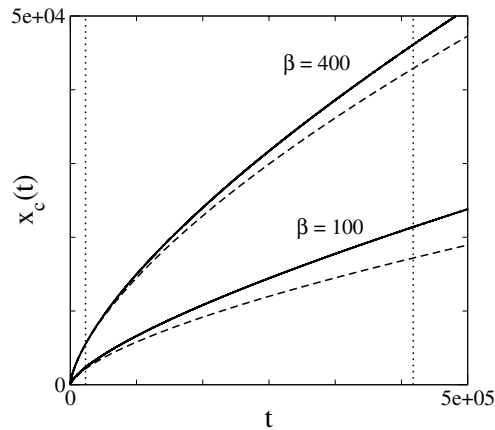
Figure 4. Comparison of the evolution of the dewetting front for a finite slip length, i.e. mobility $m(h) = h^3 + \beta h^2$ (solid curves) to the (unscaled) slip-dominated case, i.e. mobility $m(h) = \beta h^2$ (dashed curves). The choice for the slip length β is indicated on the graph for each pair of curves.

the $h_\infty = 4h_{ref}$ by $4^{1/3}$ the result collapses onto the line for $h_\infty = h_{ref}$, as required by the $h_\infty^{-1/3}$-dependence in (14).

Furthermore, we can compare the prefactors in (14) with those obtained from our fittings for the case $h_\infty = h_{ref} = 20.8$. Inserting the previously computed value for θ_s into (14) yields $x_c(t) = 0.0583t^{2/3}$; we compare this factor to the values for a_1 obtained from our fits. From the fit of (10) we get $a_1 = 0.0716$. This is only about 25% off the predictions, which is quite satisfactory if one takes into account that derivation of (14) in [2] includes scaling arguments and other approximations that make the resulting accuracy (regarding prefactors) hard to predict.

Finally, we turn to the model (9) using the nonlinear expression for curvature. In the slip-dominated case, the impact on the evolution of the dewetting front appears to be very small. In figure 3(b), the numerical results lie very close to their counterparts for the model (6) with linearized curvature, as can be seen by comparing the solid and dashed curves with the dotted curves. Consequently, the results for the fit produce values that are close to the former values; for $h_\infty = h_{ref}$, we obtain $\lambda = 0.661$ and $a_1 = 0.0739$. Finally, rescaling the graph for $x_c(t)$ for $h_\infty = h_{ref}$ (dashed curve in figure 3(b)) by $4^{1/3}$ yields a curve that coalesces with the curve for $h_\infty = h_{ref}$ (solid curve).

3.3. Finite slip length

In realistic experiments, slippage occurs for a finite slip length β. Since in the mobility $m(h) = h^3 + \beta h^2$ the second term dominates the first when $h \ll \beta$, we expect to find the typical dewetting $t^{2/3}$ law when the film profile is everywhere much smaller than the slip length. On the other hand, as the ridge grows and its height becomes of the order of, and eventually larger than, the slip length, we expect the evolution of $x_c(t)$ to increasingly depart from the $t^{2/3}$ law. Figure 4 compares the numerical results for two choices of finite β with the corresponding evolution of $x_c(t)$ using the mobility $m(h) = \beta h^2$ for the slip-dominated case. Note that for the comparison it is convenient to use this form for the mobility where β has not been removed by a rescaling of time.

Indeed, in both cases, the solid lines agree well with the dashed lines for early times but deviate at larger times. Also, for the case of larger slip length, the relative deviation increases more slowly. To make a quantitative statement, we record the deviation of the slip-dominated

evolution of x_c from the finite slip evolution when the height of the ridge is equal to the slip length. The times at which this occurs are indicated in the figure by the vertical dotted lines, the left corresponding to the lower pair of lines and $\beta = 100$, the right to the upper pair and hence $\beta = 400$. The relative deviations are quite close, in that the deviations of the front positions from the finite slip evolution are in the range of 7–7.5% for the two choices of β. We conclude that indeed the ratio of slip length and typical scale of the ridge height determines when the transition from a slip-dominated to a no-slip front evolution occurs.

A fitting ansatz for the intermediate case between no-slip and slip-dominated contact line evolution is derived by Jacobs *et al* in [7] by adding the separate contributions for the contact line velocity and then integrating the arising ODE, without detailing how their parameters relate to the slip length β. For future studies, it would be interesting to derive a dewetting law for the finite slip length case that clarifies how the slip length quantitatively determines the transition from a slip-dominated to a no-slip regime for the growing ridge. This could then be used to reconstruct the slip length from measurements of the contact line evolution.

4. Conclusions

In this paper, we revisit the evolution laws for dewetting fronts at the receding capillary ridges that form in situations where a thin polymer liquid dewets from a (very) hydrophobic substrate, and compare them to our numerical results for a lubrication and an extended lubrication model. We find that these laws capture the essence of the evolution, even quantitatively, quite well.

Our interest in these questions was spurred by the suggestion by Reiter and Sharma in [19] that slippage plays a role in the appearance of finger-like protrusions at the contact line. Their rationale can be summarized as follows: the different dewetting behaviour of ridges in the no-slip and the slip-dominated case indicate that the dewetting rate in the latter case significantly decreases as the width (and height) of the ridge increases, while in the no-slip case the dewetting rate is approximately independent of the size of the ridge. Now consider a perturbation of the ridge in the spanwise (i.e. y-) direction, giving rise to thinner and thicker parts along the contact line. Then, one would expect the thinner parts to dewet faster, while the thicker parts stay behind, thus reinforcing the pattern.

In another paper [9], we focus on this issue and use the two-dimensional form of the lubrication model (9) to investigate how spanwise perturbations evolve together with the dewetting of the ridge. Similarly as in this paper, we distinguish the asymptotic cases of no-slip ($m(h) = h^3$) and slip-dominated mobility ($m(h) = h^2$). We are first led to consider a somewhat non-standard linear stability analysis, since the base state, i.e. the dewetting ridge, is non-stationary. This analysis reveals that, both for the no-slip and slip-dominated cases, perturbations of the ridge are amplified, but the effect is greater by orders of magnitude in the slip-dominated case. Furthermore, the perturbations become asymmetrical for the slip-dominated mobility, while they develop symmetrical bulges under no-slip conditions. Additional computations that solve the two-dimensional lubrication model confirm that these findings carry over into the nonlinear regime. In this paper a comparison of our theoretical results and experiments of dewetting polystyrene on hydrophobic substrates is made. The experiments showed the formation of finger-like protrusions for polymers of different molecular weight well below the entanglement length. In striking accordance with the observed asymmetry of the perturbations in the numerical simulations, the finger-like protrusions only grow on the side of the ridge facing the hole, while the back side of the ridge remains almost flat.

The potential that applies to the liquids and substrates in the experiments in [9] is the same as the one studied in the current paper, which leads to a large length scale ratio $\rho = H/L$. Therefore, we also consider, in a further article [10], the extended lubrication model that includes the full nonlinear expression of curvature, i.e. the two-dimensional form of (9).

Acknowledgments

The author thanks Chiara Neto, Karin Jacobs, Ralph Seemann, Barbara Wagner, Tom Witelski, Ralph Blossey and John King for helpful discussions.

References

[1]   Becker J, Grün G, Seemann R, Mantz H, Jacobs K, Mecke K R and Blossey R 2003 Complex dewetting scenarios captured by thin-film models *Nat. Mater.* **2** 59–63
[2]   Brochard-Wyart F, de Gennes P-G, Hervert H and Redon C 1994 Wetting and slippage of polymer melts on semi-ideal surfaces *Langmuir* **10** 1566–72
[3]   Ghatak A, Khanna R and Sharma A 1999 Dynamics and morphology of holes in dewetting of thin films *J. Colloid Interface Sci.* **212** 483–94
[4]   Glasner K B and Witelski T P 2003 Coarsening dynamics of dewetting films *Phys. Rev.* E **67** 016302
[5]   Greenspan H P 1978 On the motion of a small viscous droplet that wets a surface *J. Fluid Mech.* **84** 125–43
[6]   Herminghaus S, Seeman R and Jacobs K 2002 Generic morphologies of viscoelastic dewetting fronts *Phys. Rev. Lett.* **89** 56101
[7]   Jacobs K, Seemann R, Schatz G and Herminghaus S 1998 Growth of holes in liquid films with partial slippage *Langmuir* **14** 4961–3
[8]   Konnur R, Kargupta K and Sharma A 2000 Instability and morphology of thin liquid films on chemically heterogeneous substrates *Phys. Rev. Lett.* **84** 931–4
[9]   Münch A, Neto C, Seemann R and Jacobs K 2004 Fingering instability in dewetting films induced by slippage, to be submitted (A partial preprint containing only the numerical results has been published on the preprint server of the DFG Research Center FZT 86 at https://www.math.tu-berlin.de/~docserv/docinfo.cgi?id=151)
[10] Münch A and Wagner B 2004 Contact line instability of dewetting thin films *Physica* D at press
[11] Neto C and Jacobs K 2004 Dynamics of hole growth in dewetting polystyrene films *Physica* A **339** 66–71
[12] Neto C, Jacobs K, Seemann R, Blossey R, Becker J and Grün G 2003 Satellite hole formation during dewetting: experiment and simulation *J. Phys.: Condens. Matter* **15** 3355–66
[13] Onogi S, Masuda T and Kitagawa K 1970 Rheological properties of anionic polystyrenes. i. dynamic viscoelasticity of narrow-distribution polystyrenes *Macromolecules* **3** 109–16
[14] Oron A, Davis S H and Bankoff S G 1997 Long-scale evolution of thin liquid films *Rev. Mod. Phys.* **69** 931–80
[15] Redon C, Brochard-Wyart F and Rondelez F 1991 Dynamics of dewetting *Phys. Rev. Lett.* **66** 715–8
[16] Redon C, Brzoska J B and Brochard-Wyart F 1994 Dewetting and slippage of microscopic polymer films *Macromolecules* **27** 468–71
[17] Reiter G 1992 Dewetting of thin polymer films *Phys. Rev. Lett.* **68** 75–8
[18] Reiter G and Khanna R 2000 Kinetics of autophobic dewetting of polymer films *Langmuir* **16** 6351–7
[19] Reiter G and Sharma A 2001 Auto-optimization of dewetting rates by rim instabilities in slipping polymer films *Phys. Rev. Lett.* **80** (16)
[20] Reiter G, Sharma A, Casoli A, David M-O, Khanna R and Auroy P 1999 Thin film instability induced by long-range forces *Langmuir* **15** 2551–8
[21] Seeman R, Herminghaus S and Jacobs K 2001 Shape of a liquid front upon dewetting *Phys. Rev. Lett.* **87** 196101
[22] Seemann R, Herminghaus S and Jacobs K 2001 Dewetting patterns and molecular forces: a reconciliation *Phys. Rev. Lett.* **86** 5534–7
[23] Seemann R, Herminghaus S and Jacobs K 2001 Gaining control of pattern formation of dewetting films *J. Phys.: Condens. Matter* **13** 4925–38
[24] Sharma A and Khanna R 1996 Nonlinear stability of microscopic polymer films with slippage *Macromolecules* **29** 6959–61
[25] Sharma A and Khanna R 1998 Pattern formation in unstable thin liquid films *Phys. Rev. Lett.* **81** 3463–6
[26] Sharma A and Khanna R 1999 Pattern formation in unstable thin liquid films under influence of antagonistic short- and long-range forces *J. Chem. Phys.* **110** 4929–36
[27] Teletzke G F, Davis H T and Scriven L E 1987 How liquids spread on solids *Chem. Eng. Commun.* **55** 41–81
[28] Xie R, Karim A, Douglas J F, Han C C and Weiss R A 1998 Spinodal dewetting of thin polymer films *Phys. Rev. Lett.* **81** 1251–4